AFRL-ML-WP-TP-2004-406

EFFECT OF INTERFACES AND THE SPIN-ORBIT BAND ON THE BAND GAPS OF InAs/GaSb SUPERLATTICES BEYOND THE STANDARD ENVELOPE-FUNCTION APPROXIMATION

F. Szmulowicz, H. Haugan, and G.J. Brown

Sensors Materials Branch (AFRL/MLPS)
Survivability and Sensor Materials Division
Materials and Manufacturing Directorate
Air Force Research Laboratory, Air Force Materiel Command
Wright-Patterson AFB, OH 45433-7750

April 2004

Approved for public release; distribution is unlimited.

STINFO FINAL REPORT

MATERIALS AND MANUFACTURING DIRECTORATE
AIR FORCE RESEARCH LABORATORY
AIR FORCE MATERIEL COMMAND
WRIGHT-PATTERSON AIR FORCE BASE, OH 45433-7750

NOTICE

Using government drawings, specifications, or other data included in this document for any purpose other than government procurement does not in any way obligate the U.S. Government. The fact that the government formulated or supplied the drawings, specifications, or other data does not license the holder or any other person or corporation; or convey any rights or permission to manufacture, use, or sell any patented invention that may relate to them.

This report has been reviewed by the AFRL Wright Site Office of Public Affairs (WS/PA) and is releasable to the National Technical Information Service (NTIS). At NTIS, it will be available to the general public, including foreign nationals.

This technical report has been reviewed and is approved for publication.

//s//

Pamela M. Schaefer
Principal Materials Engineer
Technical & Strategic Planning Office
Materials and Manufacturing Directorate

Copies of this report should not be returned unless return is required by security considerations, contractual obligations, or notice on a specific document.

REPORT DOCUMENTATION PAGE

Form Approved
OMB No. 0704-0188

1. REPORT DATE *(DD-MM-YY)*	2. REPORT TYPE	3. DATES COVERED *(From - To)*
April 2004	Journal article	

4. TITLE AND SUBTITLE
EFFECT OF INTERFACES AND THE SPIN-ORBIT BAND ON THE BAND GAPS OF INAS/GASB SUPERLATTICES BEYOND THE STANDARD ENVELOPE-FUNCTION APPROXIMATION

5a. CONTRACT NUMBER
IN-HOUSE

5b. GRANT NUMBER

5c. PROGRAM ELEMENT NUMBER
N/A

6. AUTHOR(S)
F. Szmulowicz, H. Haugan, and G.J. Brown

5d. PROJECT NUMBER
M07R

5e. TASK NUMBER
10

5f. WORK UNIT NUMBER
00

7. PERFORMING ORGANIZATION NAME(S) AND ADDRESS(ES)
Sensors Materials Branch (AFRL/MLPS)
Survivability and Sensor Materials Division
Materials and Manufacturing Directorate
Air Force Research Laboratory, Air Force Materiel Command
Wright-Patterson Air Force Base, OH 45433-7750

8. PERFORMING ORGANIZATION REPORT NUMBER
AFRL-ML-WP-TP-2004-406

9. SPONSORING/MONITORING AGENCY NAME(S) AND ADDRESS(ES)
Materials and Manufacturing Directorate
Air Force Research Laboratory
Air Force Materiel Command
Wright-Patterson Air Force Base, OH 45433-7750

10. SPONSORING/MONITORING AGENCY ACRONYM(S)
AFRL/MLPS

11. SPONSORING/MONITORING AGENCY REPORT NUMBER(S)
AFRL-ML-WP-TP-2004-406

12. DISTRIBUTION/AVAILABILITY STATEMENT
Approved for public release; distribution is unlimited.

13. SUPPLEMENTARY NOTES
Published in *Physical Review B*, 69, 155321 (2004).

ABSTRACT ***(Maximum 200 Words), ,***
We developed a modified 8x8 envelope-function approximation (EFA) formalism for the noncommon-atom (NCA) superlattices (SL's), incorporating the effect of anisotropic and other interface (IF) interactions that go beyond the standard EFA. The boundary condition in the presence of IF interactions are used to set up a secular equation (including a transfer matrix derivation) whose physical transparency makes possible a number of valuable insights (possibility of IF bound states, analytic solutions, indirect gaps, etc.). We show that the heavy-hole-spin-orbit IF coupling is very important due to the IF localization of the SO wave function components and the ability of the IF potential to potentially bind a hole at the IF's, all of which pose convergence problems for perturbative solutions. With two adjustable parameter for the two possible IF's, we find a very good agreement between experiment and theory for the band gaps of several sets of very long-infrared and midinfrared InAs/GaSb SL's grown at several laboratories and by us. The band gaps as a function of GaSb and InAs widths are explained in terms of variations of the HH and conduction (*C*) bandwidths.

15. SUBJECT TERMS

16. SECURITY CLASSIFICATION OF:			17. LIMITATION OF ABSTRACT:	18. NUMBER OF PAGES	19a. NAME OF RESPONSIBLE PERSON (Monitor)
a. REPORT	b. ABSTRACT	c. THIS PAGE			Gail J. Brown
Unclassified	Unclassified	Unclassified	SAR	24	19b. TELEPHONE NUMBER *(Include Area Code)* (937) 255-4474, ext. 3238

Standard Form 298 (Rev. 8-98)
Prescribed by ANSI Std. Z39-18

PHYSICAL REVIEW B 69, 155321 (2004)

Effect of interfaces and the spin-orbit band on the band gaps of InAs/GaSb superlattices beyond the standard envelope-function approximation

F. Szmulowicz, H. Haugan, and G. J. Brown
Air Force Research Laboratory, Materials and Manufacturing Directorate, Wright-Patterson AFB, Ohio 45433-7707, USA
(Received 26 November 2003; revised manuscript received 26 January 2004; published 22 April 2004)

We develop a modified 8×8 envelope-function approximation (EFA) formalism for the noncommon-atom (NCA) superlattices (SL's), incorporating the effect of anisotropic and other interface (IF) interactions that go beyond the standard EFA. The boundary conditions in the presence of IF interactions are used to set up a secular equation (including a transfer matrix derivation) whose physical transparency makes possible a number of valuable insights (possibility of IF bound states, analytic solutions, indirect gaps, etc.). We show that the heavy-hole–spin-orbit IF coupling is very important due to the IF localization of the SO wave function components and the ability of the IF potential to potentially bind a hole at the IF's, all of which pose convergence problems for perturbative solutions. With two adjustable parameter for the two possible IF's, we find a very good agreement between experiment and theory for the band gaps of several sets of very long-infrared and midinfrared InAs/GaSb SL's grown at several laboratories and by us. The band gaps as a function of GaSb and InAs widths are explained in terms of variations of the HH and conduction (C) band bandwidths. We show that the cut-off wavelengths can be reduced by increasing the GaSb layer width. Thus, a consistent application of the EFA method with the inclusion of well established IF effects can provide useful physical insights and possesses good predictive capacity in the design of NCA SL's.

DOI: 10.1103/PhysRevB.69.155321 PACS number(s): 78.66.−w, 78.66.Fd, 07.57.Kp, 42.55.Px

I. INTRODUCTION

InAs/InGaSb superlattices (SL's) have been proposed by Smith and Mailhiot[1,2] and grown by many groups for use as detectors and lasers operating in the short to very long infrared wavelength regions.[3–5] This SL system has been modeled using a variety of computational approaches,[6–32] including the popular envelope-function approximation (EFA) method. Recently, however, problems with the numerical accuracy of the standard EFA in the case of InAs/GaSb binary-binary superlattices have been reported.[8,14,21] For example, Northwestern Sample No. 1303—$(InAs)_{17}/(GaSb)_4$ with InSb IF's (Ref. 12)—was measured to have the cutoff of about 30 μm whereas our standard 8×8 EFA code[32] predicts a 5.5 μm cutoff. Another Northwestern SL—$(InAs)_{17}/(GaSb)_7$ with InSb IF's—has the cutoff of 19 μm,[11] whereas our standard 8×8 EFA predicts a 7.5 μm cutoff. In our EFA simulations, changing the layer widths by one monolayer, varying band offsets by ±10 meV, and even relaxing the SL did not change the cutoff by more than 1 μm.

The standard EFA encounters the same problem for mid-IR InAs/GaSb SL's. For example, Kaspi *et al.*[23] grew a series of SL's and measured their absorption cutoffs as a function of GaSb width. In disagreement with Kaspi's data, the standard 8×8 EFA model does not predict large changes in the band gap. Whereas the EFA calculated band gaps for InAs/GaSb SL's varying from 6 ML/6 ML to 6 ML/24 ML increase from 421 to 452 meV, absorption and PL data indicate that the gaps increase more rapidly from about 320 to 430 meV.[22,23] The larger error for the thinner SL suggests a correspondingly greater role of the IF's. Similarly, in the series of InAs/GaSb SL samples ranging from 8 ML/8 ML to 8 ML/40 ML, the band gaps via the standard EFA range from 343 to 352 meV, whereas absorption/PL data range from (277/263) to (352/353) meV,[22] with disagreement again increasing for thinner SL's.

This disagreement motivated us to reexamine the standard EFA model.[33,34] Recently, the standard EFA has been expanded to model IF anisotropy in NCA SL's (Refs. 35–39) and used to account for their giant absorption anisotropy. In III-V heterojunctions with noncommon anions or cations, grown in the [001] direction, adjacent rows of atoms are at right angles to each another, so that the true IF symmetry is C_{2v} rather than D_{2d} as assumed in the standard EFA.[35] The lowering of the symmetry causes heavy-hole–light-hole (HH-LH) interaction even at the center of the Brillouin zone (BZ), point $\bar{\Gamma}$. Using the theory of invariants,[40,41] Ivchenko, Kaminski, and Rössler[42] showed that the form of the IF interaction is the consequence of the symmetry of SL's with NCA IF's and modeled it with a short-range delta function potential centered at the IF's.[42–46] Foreman[47] than formally justified the use of short range IF potentials to model IF effects at NCA IF's using Burt's EFA representation.[48] Takhtamirov and Volkov[49–52] used a simple model of an IF to relate the IF parameters to IF grading and derived a more general form of the IF potential within the EFA.

In a number of papers, the theory of Refs. 35–39 has been applied using the perturbative $\mathbf{k}\cdot\mathbf{P}$ EFA approach to model band gap data and to explain spin relaxation experiments.[28–31] In Lau *et al.*,[30] both the $\mathbf{k}\cdot\mathbf{P}$ term and the IF effects are treated as a perturbation on the "unperturbed" SL bands at $\bar{\Gamma}$ and the HH-SO IF coupling (see Refs. 43, 52) is not included. The EFA $\mathbf{k}\cdot\mathbf{P}$ method in conjunction with the IF Hamiltonian of Krebs and Voisin[35] (labeled H_{BF}) demonstrated improved agreement with data.[22,23]

Wang *et al.*[14] and Magri *et al.*[15–19] critically explored the limits of the EFA in specific applications by comparison to the more numerically intensive empirical pseudopotential

(EPS) calculations. For example, Magri *et al.*[19] show that the standard EFA and EPS calculations agree if the EFA input parameters come from the same EPS band structure calculation. The electronic structure of InAs/GaSb SL's has also been calculated via the superlattice empirical pseudopotential method (SEPM).[22–26] Unlike the EPS,[17] the SEPM (Ref. 26) assumes that IF's remain sharp and bulklike, so that the method does not differentiate between different types of bonds possible at interfaces. Nevertheless, good agreement is found with experimental absorption data[23,26] on the band gaps for a series of samples.[22,23]

In the more accurate atomic EPM (AEPM) model,[14–19] the pseudopotential is fitted to bulk bands and effective masses, and the spin-orbit interaction is included via the nonlocal part of the pseudopotential. An adjustable scale factor multiplies the kinetic energy operator for better fits to the bulk band gap data and to the momentum matrix coupling the valence and conduction bands. Without additional information on the atomic detail of the IF's, the AEPM (Ref. 14) has limited success in predicting the correct band gap trends with layer thickness.[26] Indeed, AEPM (Ref. 27) can predict wrong dependence of InAs/GaSb band gaps on GaSb layer thickness.[26] However, Magri *et al.* found a very good agreement with experimental band gaps for a series of InAs/GaSb SL's via EPM by accounting for interfacial diffusion.[17]

EPS and EFA represent two valid paths to the goal of modeling heterostructures. EFA has greater physical appeal, is vastly less computationally intensive in its setup and execution, can be more readily implemented by a nonspecialist, and is more easily used for calculations involving electric and magnetic fields, Auger lifetimes, ionization coefficients, etc. The EPS directly accounts for all possible interface bonds and, given an atomic model of interdiffusion, it can model interdiffused IF's. The present EFA models these effects through powerful symmetry arguments about the form of the IF potential. If atomic profiles are known either experimentally[54,55] or theoretically,[17] they may be included in the EFA as explained in Ref. 47 or Refs. 50–53.

In this paper, we investigate NCA IF effects within a modified 8×8 EFA by solving the EFA Hamiltonian nonperturbatively, based on the solution of the relevant boundary conditions (BC approach). We adopt the IF Hamiltonian of Ivchenko, Kaminski, and Rössler[42] and that of Takhtamirov and Volkov,[52] including the IF coupling to the SO band.[43,52] This paper is organized as follows. Section II provides a summary of existing approaches to the problem of representing IF's in the EFA. Next, in Sec. III, the solution of the problem is formulated using the numerically stable representation of the secular equation in terms of tangents only, which is algorithmically simple and guards against the occurrence of large exponentials.[32] This method also affords a number of physical insights into the influence of IF's on the electronic structure of SL's and the large role of the SO band. We find that the IF coupling of the HH band to the SO is very important in spite of the large SO splitting in InAs/GaSb SL's. This is so because the SO wave function is concentrated at the IF's and is further admixed by the LH-SO interaction in the $\mathbf{k}\cdot\mathbf{p}$ Hamiltonian at $\bar{\Gamma}$. Further, because of the singular nature of the perturbation introduced by the IF's, we show that the problem cannot be dealt with perturbatively since the solutions of the unperturbed problem cannot represent the rapidly evanescent components of the wave function at the IF's. We demonstrate this by performing a 14-band perturbative $\mathbf{k}\cdot\mathbf{P}$ EFA calculation with the IF interaction as the perturbation.

In Sec. IV, we compare the results of the present calculation to the band gap data from several laboratories, including ours.[56] We explain the band gaps as a function of GaSb and InAs widths in terms of variations of the heavy-hole and conduction band bandwidths. We show that the cutoff wavelengths can be reduced by increasing the GaSb layer thickness. Conclusions are presented last in Sec. V.

II. REVIEW OF INTERFACE REPRESENTATION IN EFA

For noncommon-atom III/V IF's, [110] and [−110] directions are inequivalent, not being connected by a fourfold rotoinversion operation IC_{4z}, so that the symmetry at a single IF is reduced from D_{2d} to C_{2v}.[6,7] As a result, the z component of the total angular momentum J_z is no longer a good quantum number so that HH and LH are coupled even at $\bar{\Gamma}$. To first order, the S-like conduction electrons are unaffected. The EFA representation of Burt deals with the validity of EFA in the IF regions.[47,48] Here, three extensions of the theory to IF effects in the EFA are described.

A. Krebs and Voisin

Krebs and Voisin[35] showed that the giant in-plane optical anisotropy of NCA group-III SL's can be explained by the reduction of the assumed D_{2d} symmetry to the C_{2v} symmetry. Using bond counting arguments, they showed that the resulting symmetry reduction couples the light and heavy bands even at $\bar{\Gamma}$, unlike in the standard EFA.[33,34] The effect can be modeled in the EFA via a short-range (δ) potential at SL IF's.[42,52] The short range of the interaction in the EFA was subsequently proved rigorously by Foreman[47] and Takhtamirov and Volkov.[52] However, the Krebs-Voisin theory contains diagonal HH-HH and LH-LH coupling with the same coupling constant as the HH-LH coupling. Such coupling does not appear in the theory of Ivchenko *et al.*[42–46] and, in the theory of Takhtamirov and Volkov,[49–52] it is present only for nonabrupt IF's as an isotropic interaction with an unrelated coupling constant. Recently, Krebs-Voisin theory was used to calculate the hole-spin relaxation times and absorption spectra in InAs/GaSb SL's.[28–30] The strengths of the anisotropic IF interactions (one for each IF type) in the theory were fit to the experimental values of the hole-spin relaxation times and band gap energies.

B. Ivchenko, Kaminski, and Rössler

Ivchenko, Kaminski, and Rössler[42] represented the effect of IF anisotropy on the EFA Hamiltonian based on the theory of invariants in which the Hamiltonian is expanded in a series of operators that are invariant under the symmetry operations of the system.[40,41] The value of the expansion coefficients is fixed by experiments but the form of the Hamiltonian is governed by the symmetry of the system.[57,58]

We adopt the form of the IF Hamiltonian that is given by[42,52]

$$V = H_{XY} a_0 \delta(z) \Theta, \tag{1a}$$

where in the $|JM_J\rangle$ basis

$$\Theta = \begin{pmatrix} 0 & 0 & i/\sqrt{3} & 0 & 0 & \sqrt{2/3} \\ 0 & 0 & 0 & i/\sqrt{3} & 0 & 0 \\ -i/\sqrt{3} & 0 & 0 & 0 & 0 & 0 \\ 0 & -i/\sqrt{3} & 0 & 0 & \sqrt{2/3} & 0 \\ 0 & 0 & 0 & \sqrt{2/3} & 0 & 0 \\ \sqrt{2/3} & 0 & 0 & 0 & 0 & 0 \end{pmatrix} \tag{1b}$$

and the $|JM_J\rangle$ basis is arranged in the order $|\frac{3}{2},\frac{3}{2}\rangle$, $|\frac{3}{2},\frac{1}{2}\rangle$, $|\frac{3}{2},-\frac{1}{2}\rangle$, $|\frac{3}{2},-\frac{3}{2}\rangle$, $|\frac{1}{2},\frac{1}{2}\rangle$, $|\frac{1}{2},-\frac{1}{2}\rangle$, a_0 is a lattice constant (here, that of GaSb), and H_{XY} is the strength of the IF potential. The interaction potential in Eq. (1a) contains HH-LH and HH-SO coupling and no diagonal HH-HH or LH-LH terms, so that the H_{BF} description of Krebs and Voisin[35,38] is not equivalent to that of Ivchenko *et al.*[42] It is also common to use the dimensionless coupling parameter t, defined through $H_{XY} = \hbar^2 t / 2 m_0 a_0^2$.

C. Takhtamirov and Volkov

Takhtamirov and Volkov[50–52] adopt a particular model of IF interaction in order to derive an EFA Hamiltonian with IF effects. In their model, the EFA potential $U(\mathbf{r})$ across a single AB IF is graded as[52]

$$U(\mathbf{r}) = U_A(\mathbf{r}) + G(\mathbf{r})[U_B(\mathbf{r}) - U_A(\mathbf{r})], \tag{2}$$

and all IF-related parameters are expressed in terms of the Fourier harmonics (form factors) of $G(\mathbf{r})$ and $U_B(\mathbf{r}) - U_A(\mathbf{r})$ [see Eq. (25) of Ref. 52], where $G(\mathbf{r})$ is a grading function periodic in the in-plane direction. As such, the theory contains no *ad hoc* adjustable parameters for the strength of the IF interaction. This theory naturally introduces diagonal band coupling for nonabrupt IF's, which become important for valence and conduction bands in narrow wells. In the limit of sharp IF's, the theory of Takhtamirov and Volkov reduces to that of Ivchenko, Kaminski, and Rössler, Eqs. (1a) and (1b).

III. FORMALISM DEVELOPMENT OF THE MODIFIED EFA THEORY

This section develops the mathematical formalism for the modified EFA theory, an EFA theory that includes IF effects nonperturbatively through the boundary conditions.

A. Hamiltonian

The notation used in this paper is consistent with that used previously.[32] The superlattice consists of alternating layers of material A (say, GaSb) of width $2a$ and material B (here, InAs) of width $2b$. In the zeroth unit cell, material A ranges between $(b < z \leq b + 2a)$ and material B between $(-b < z \leq b)$. The period $d = 2a + 2b$.

In each layer of a heterostructure, the $N \times N$ EFA Hamiltonian (here, $N = 2 \times 4 = 8$) is expanded in powers of k_z (Refs. 32, 58, and 59)

$$H(\mathbf{k}_\parallel, k_z) = k_z H_2(\mathbf{k}_\parallel) k_z + [H_1(\mathbf{k}_\parallel) k_z + k_z H_1(\mathbf{k}_\parallel)]/2 + H_0(\mathbf{k}_\parallel), \tag{3}$$

where $k_z = -id/dz$ and $H_0(\mathbf{k}_\parallel)$, $H_1(\mathbf{k}_\parallel)$, and $H_2(\mathbf{k}_\parallel)$ are Hermitian and z dependent;[59] strain is included as described before.[32] At IF's $z = \pm b$, there are additional IF-localized terms (1a),

$$V = [H_{XY}^{BA} a_0 \delta(z-b) - H_{XY}^{AB} a_0 \delta(z+b)] \Theta. \tag{4}$$

For InAs/GaSb SL's, there are two possibly different IF's—the BA interface GaSb-on-InAs at $z = b$ and the AB interface InAs-on-GaSb at $z = -b$—either of which can be grown InSb-like or GaAs-like. In practice, IF's often turn out to be mixed and interdiffused, depending on growth conditions and degree of growth control.[54,55] For very thin SL's, a scalar diagonal IF interaction may become important[52] and may be easily incorporated in the present theory.[60]

Away from IF's in each layer of the SL, the EFA Schrödinger equation for the envelope functions F (an N vector) is given by[32]

$$\frac{d^2F}{dz^2} + i(H_2)^{-1} H_1 \frac{dF}{dz} - (H_2)^{-1}(H_0 - E)F = 0 \tag{5}$$

and the solutions have the form

$$F_v(\mathbf{k}_\parallel, q, z) = \sum_{i=1}^{2N} C_v(\mathbf{k}_\parallel, k_i) \exp(i k_i z) c_i(\mathbf{k}_\parallel, q), \tag{6}$$

where the N vector $C_v(\mathbf{k}_\parallel, k_i)$ is the right eigenvector[59] of

$$(H_2 k^2 + H_1 k + H_0) C = E C \tag{7}$$

at energy E and exponents k_i $(i = 1, \ldots, 2N)$ are the roots of the determinental equation

$$\| H_2 k^2 + H_1 k + (H_0 - E) \| = 0. \tag{8}$$

In matrix notation, the column vector for the envelope function, (6) is given by

$$F(z) = C \exp(iKz) c, \tag{9}$$

where $K_{ij} = k_i \delta_{ij}$, so that the exponential matrix is also diagonal

$$[\exp(iKz)]_{ij} = \exp(k_i z)\, \delta_{ij}. \tag{10}$$

B. Boundary conditions

At interfaces, EFA requires the continuity of the envelope function and current.[32,33,59] In absence of IF effects, the two continuity conditions require the continuity of the following compact expression:[32]

$$\begin{pmatrix} 1 & 0 \\ iH_1/2 & H_2 \end{pmatrix}\begin{pmatrix} F \\ F' \end{pmatrix} \tag{11a}$$

or, equivalently, of

$$M\exp(iKz)c, \tag{11b}$$

where the material-dependent matrix M is given by

$$M=\begin{pmatrix} I & 0 \\ H_1/2 & H_2 \end{pmatrix}\begin{pmatrix} C \\ CK \end{pmatrix}. \tag{12}$$

At $z=b$, integrating the Hamiltonian across the BA interface, the two boundary conditions become

$$(I+i\Phi_{BA})M_A\exp(iK_Ab)c_A=M_B\exp(iK_Bb)c_B, \tag{13a}$$

which can be written as

$$\exp(i\Phi_{BA})M_A\exp(iK_Ab)c_A=M_B\exp(iK_Bb)c_B, \tag{13b}$$

where the addition of the δ-function interaction terms at the IF gives rise to a phase factor $\exp(i\Phi_{BA})$ with the "phase angle" defined through the interface matrix

$$\Phi_{BA}\equiv H_{XY}^{BA}a_0\begin{pmatrix} 0 & 0 \\ \Theta & 0 \end{pmatrix}. \tag{14}$$

Appendix A lists the properties of the interface matrix and of the exponential $\exp(i\Phi)$.

At the AB interface $z=-b$, the boundary conditions augmented by the Bloch periodicity condition, can be written as

$$\exp(-iqd)\exp(i\Phi_{AB})M_A\exp[iK_A(d-b)]c_A = M_B\exp(-iK_Bb)c_B, \tag{15}$$

where the strength of the IF term is $\Phi_{AB}\equiv H_{XY}^{AB}a_0\left(\begin{smallmatrix} 0 & 0 \\ \Theta & 0 \end{smallmatrix}\right)$. For symmetric IF's, $H_{XY}^{AB}=H_{XY}^{BA}$ in Eq. (4).

C. Secular equation and solution

The two boundary conditions can be solved simultaneously to yield the equation

$$[\exp(i\Phi_{AB})\exp[2i(\Lambda_Aa-qd/2)] - \exp[-2i\Lambda_Bb]\exp(i\Phi_{BA})]\Gamma=0, \tag{16}$$

where the eigenvector can be expressed as

$$\Gamma=\exp(-i\Phi_{BA})\exp(i\Lambda_Bb)M_Bc_B \tag{17}$$

or as

$$\Gamma=\exp(i\Lambda_Ab)M_Ac_A; \tag{18}$$

therefore, Γ can be used to find both c_A and c_B. The Λ matrices are defined via

$$\exp(i\Lambda_Aa)\equiv M_A\exp(iK_Aa)M_A^{-1}. \tag{19}$$

Although Eq. (16) can serve perfectly well as a secular equation, it contains exponentials that might become very large for complex exponents (evanescent solutions). Instead, we define $A\equiv\tan(\Lambda_Aa-qd/2)$ and $B=\tan\Lambda_Bb$ and use the general operator identity[61]

$$\exp(2i\Sigma)=(1+i\tan\Sigma)/(1-i\tan\Sigma) \tag{20}$$

and obtain two equivalent equations secular for matrices Ω_1 and Ω_2

$$[-i(1-iB)\exp(i\Phi_{BA})(1-iA)+i(1+iB)\exp(i\Phi_{AB}) \times(1+iA)]X\equiv\Omega_1X=0, \tag{21}$$

$$[-i(1-iA)\exp(-i\Phi_{AB})(1-iB)+i(1+iA)\exp(-i\Phi_{BA}) \times(1+iB)]Y\equiv\Omega_2Y=0, \tag{22}$$

with the eigenvectors

$$X=\cos(\Lambda_Aa-qd/2)\exp[i(\Lambda_A-qI)d/2]M_Ac_A, \tag{23}$$

$$Y=(\cos\Lambda_Bb)M_Bc_B. \tag{24}$$

For complex exponents, Eqs. (21) and (22) grow only as hyperbolic tangents. For a more symmetric appearance, the results are also valid with the use of $A=\tan(\Lambda_Aa-qd/4)$ and $B=\tan(\Lambda_Bb-qd/4)$. Note also that the secular equation is not a simple function of the sum or difference of the IF terms Φ_{AB} and Φ_{BA}.

The energy eigenvalues are at the zeroes of either determinant

$$\|\Omega_1\|=\|\Omega_2\|=0, \tag{25}$$

since the determinants are equal. In the absence of IF effects, Eq. (25) reduces to the simple, tangents-only form found earlier[32]

$$\|A+B\|=\|\tan(\Lambda_Aa-qd/4)+\tan(\Lambda_Bb-qd/4)\|=0. \tag{26}$$

After the zeroes of say, $\|\Omega_1\|$, are identified, the corresponding eigenvector X can be used directly to find the wave function expansion coefficient c_A via Eq. (23); then, c_B is found from

$$X=[\exp(-i\Phi_{BA})\exp(i\Lambda_Bb)+\exp(-i\Phi_{AB}) \times\exp(-i\Lambda_Bb)]M_Bc_B/2 \tag{27}$$

or, equivalently, from

$$X=\exp[-i(\Phi_{AB}+\Phi_{BA})/2]\left[I+\sin\left(\frac{\Phi_{BA}-\Phi_{AB}}{2}\right)\tan\Lambda_Bb\right] \times(M_B\cos K_Bb)c_B. \tag{28}$$

Using Ω_2 to find Y and then c_B is formally correct but doubles the computational effort.

Lastly, for symmetric IF's, $\Phi_{AB}=\Phi_{BA}\equiv\Phi$, one form of the secular equation is

$$\|\exp(i\Phi)A\exp(-i\Phi)+B\|=0. \tag{29}$$

For completeness, the secular equation can also be put in the Kronig-Penney-like form

$$\|[\exp(i\Phi_{AB})\exp(2i\Lambda_A a)\exp(-i\Phi_{BA})\exp(2i\Lambda_B b) + \exp(-2i\Lambda_B b)\exp(i\Phi_{BA})\exp(-2i\Lambda_A a) \times \exp(-i\Phi_{AB})]/2-\cos qd\| = 0. \quad (30)$$

Equations in this section can be derived using the transfer matrix approach,[62] Appendix B.

D. Symmetry

The choice of origin in the middle of layer B is arbitrary. Choosing the origin in the middle of layer A (or translating the system by half the period), shows that there is a hidden symmetry $(A,a)\leftrightarrow(B,b)$, i.e., A and B are dummy labels. For symmetric IF's, Eq. (29), changing the sign of the interaction at each IF, $\Phi\rightarrow-\Phi$, and interchanging the dummy labels $A\leftrightarrow B$ shows that the determinant is independent of the sign of the interaction. For inequivalent IF's, Eqs. (21) and (22), if the sign of the interaction at each IF is changed, $\Phi_{AB}\rightarrow-\Phi_{AB}$ and $\Phi_{BA}\rightarrow-\Phi_{BA}$, and the dummy labels $A\leftrightarrow B$ are interchanged, it is found that $\Omega_1\leftrightarrow\Omega_2$, so that the eigenvalue problem is again independent of the sign of the interaction. Appendix C provides explicit solutions for a number of analytic models of SL's with symmetric interface interactions; invariably the solutions are proportional to the square of the dimensionless coupling parameter t.

The symmetry group for a symmetric SL is D_{2d} with eight symmetry operations of $C_{2v}=\{E,C_{2z},IC_{2a},IC_{2b}\}$ augmented with four operations that interchange the two IF's IC_{4z}, $(IC_{4z})^{-1}$, C_{2y}, C_{2x}.[57] The factor group at $\bar{\Gamma}$ is D_{2d} itself, with two irreducible representations compatible with spin Γ_6 and Γ_7. Along the q axis, the factor group is C_{2v}, which has a single two-dimensional representation Γ_5, so there is no spin splitting. Along the k_x axis, the factor group is C_2 consisting of identity and a twofold rotation about the x axis, with two singly degenerate representations Γ_3 and Γ_4, so that all bands are spin split. Representations Γ_6 and Γ_7 at $\bar{\Gamma}$ decompose into Γ_3 and Γ_4 along the k_x axis.[6,7]

For an asymmetric SL, the point group symmetry is C_{2v}. The factor group at $\bar{\Gamma}$ and along the q axis is C_{2v} itself with a single double degenerate representation. And along the k_x axis, the factor group is C_1 with one singly degenerate representation so that the bands anticross.[6,7] Of course, time reversal symmetry dictates that energy bands be degenerate upon reversal of wave vector and spin.

E. Hermiticity

In Ref. 32, the following identity was proved:

$$TAT=A^+, \quad (31)$$

where the row (or column) interchange matrix is given by

$$T=\begin{pmatrix}0 & I\\ I & 0\end{pmatrix}, \quad (32)$$

which helped prove that $A+B$, Eq. (26), can be made Hermitian by interchanging its first and last N rows (or columns). Here, in addition, we find that

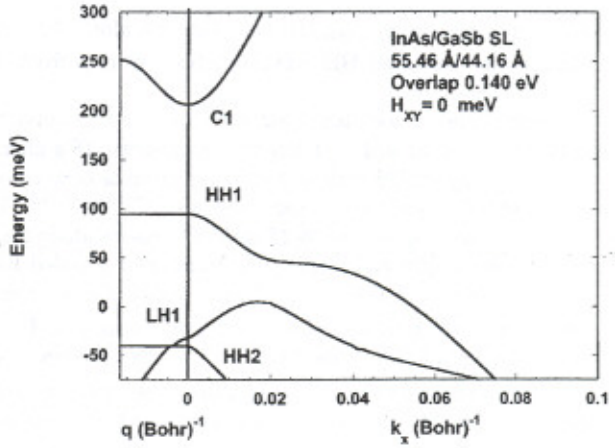

FIG. 1. The band structure of a test InAs/GaSb superlattice with 44.16 Å GaSb/55.46 Å InAs without IF effects using the standard 8×8 EFA (Ref. 32). The zero of energy is at the CB edge of bulk InAs.

$$T(I+i\Phi)T=(I-i\Phi)^+ \quad (33a)$$

or

$$T\exp(i\Phi)T=[\exp(-i\Phi)]^+. \quad (33b)$$

The same proof with the present secular equation, (21) proves that Ω_1 cannot be made Hermitian because of the IF terms. However,

$$T\Omega_1 T=\Omega_2^+; \quad (34)$$

therefore, using Eq. (25),

$$\|\Omega_1\|=\|\Omega_2\|=\|\Omega_2^+\|, \quad (35)$$

so that the determinant is real, an important consideration for numerical purposes. Lastly, it follows from Eq. (34) that if $\Omega_1 X=\lambda X$ and $\Omega_2 Y=\mu Y$ then $\lambda^*=\mu$, and

$$(TX)^+\Omega_2=\lambda^*(TX)^+. \quad (36)$$

The eigenvalue problem is best solved by diagonalizing Ω_1 as a function of energy for a given wave vector. The determinant given by the product of diagonal elements, λ_i $(1=1,...2N)$, is zero at an energy eigenvalue, and the wave vector X_j corresponding to the zero eigenvalue, $\lambda_j=0$, is used to find the envelope function, Eqs. (23) and (27).

F. Typical band structure

We adopt a test superlattice for displaying typical results of the calculation. The test structure is an InAs/GaSb SL with 44.16 Å GaSb/55.46 Å InAs and both InSb IF's. The physical input parameters are given in Table IX in Appendix D. For future comparison, the band structure of this SL without IF effects (standard EFA) is shown in Fig. 1 and has the band gap of 111.4 meV. The unstrained conduction-band–valence-band overlap is taken to be 0.140 eV for the test case. Three valence bands and one conduction band are shown. The bands labeled HH and LH do not interact at $\bar{\Gamma}$ but are hy-

bridized along the k_x axis; HH bands are flat along the q axis because of the small HH wave function overlap from one period to another.

Figure 2(a) shows the band structure of the same test InAs/GaSb SL as in Fig. 1 but with symmetric IF's characterized by $H_{XY}=525$ meV or $t=5.12$, a number on the order of magnitude used by previous workers.[28,30,37,38,42,44,50] The resulting band gap is now 96.25 meV. The bands along the k_x axis are spin split and there are a number of avoided band crossings that lead to level repulsions, among them a rise of the HH1 band, thus a smaller band gap. Starting at $\bar{\Gamma}$, the bands are split in opposite directions, so that the top of the valence band is away from $\bar{\Gamma}$, Fig. 2(b). Along the q axis, the bands are doubly degenerate, and level repulsion results in the top of the valence band being displaced from $\bar{\Gamma}$ to $\bar{L}=(0,0,\pi/d)$. Since the S-like Cl'band (not shown) is not directly coupled by the perturbation, its is largely unaffected (except through indirect coupling to LH and SO bands.)

Next, Fig. 2(c) shows the test SL with asymmetric IF's, $H_{XY}=525$ meV at one IF and $H_{XY}=0$ at the other. Along the q axis the bands are doubly degenerate and the HH1 band is much flatter than in Fig. 2(b). Along the k_x axis, the bands are spin split again and, belonging to different symmetry representations, they all repel.

In Fig. 2(b), the positive curvature of the HH1 band along the q axis requires explanation. For small q, the nondegenerate perturbation theory with the perturbation

$$\left(\frac{\hbar^2 q^2}{2m}+\frac{\hbar}{m}qp_z\right)+H_{XY}a_0[\delta(z-b)-\delta(z+b)]\Theta \quad (37)$$

(i.e., $\mathbf{k}\cdot\mathbf{p}$ and IF terms) would require fourth order terms q^2t^2. Therefore, we use $V=H_{XY}a_0[\delta(z-b)-\delta(z+b)]\Theta$ itself as the perturbation on the already calculated SL bands as a function of q. Perturbation V couples HH1 (symmetric with respect to the centers of GaSb and InAs layers) and LH2 (antisymmetric about the centers of InSb and GaSb layers) bands at the zone center. Near $\bar{\Gamma}$, we approximate the unperturbed HH1 as E^0_{HH1} (dispersionless) and LH2 as $E^0_{\mathrm{LH2}}+\hbar^2q^2/2m^0_{\mathrm{LH2}}$, where $m^0_{\mathrm{LH2}}>0$, Fig. 1, and find in first-order nondegenerate perturbation theory that

$$E_{\mathrm{HH1}}(q)=E^0_{\mathrm{HH1}}+\frac{|V_{12}|^2}{(E^0_{\mathrm{HH1}}-E^0_{\mathrm{LH2}})}+\frac{|V_{12}|^2}{(E^0_{\mathrm{HH1}}-E^0_{\mathrm{LH2}})^2}\frac{\hbar^2q^2}{2m^0_{\mathrm{LH2}}}, \quad (38)$$

where $V_{12}=\langle \mathrm{HH1}|V|\mathrm{LH2}\rangle$ and superscript zero denotes quantities evaluated at $\bar{\Gamma}$. For symmetric IF's, both IF's contribute equally to the overlap integral V_{12}. From Eq. (38) we find the following.

(a) Since $E^0_{\mathrm{HH1}}>E^0_{\mathrm{LH2}}$, interaction with the LH2 band raises the HH1 band in agreement with Fig. 2, independent of the sign of H_{XY}.

(b) HH1 band acquires some of the curvature of the LH2 band ($E^0_{\mathrm{LH2}}=-336.08$ meV). Since the LH2 band has a positive curvature along the q axis, the dispersionless HH1 band also acquires positive curvature, Fig. 2(b).

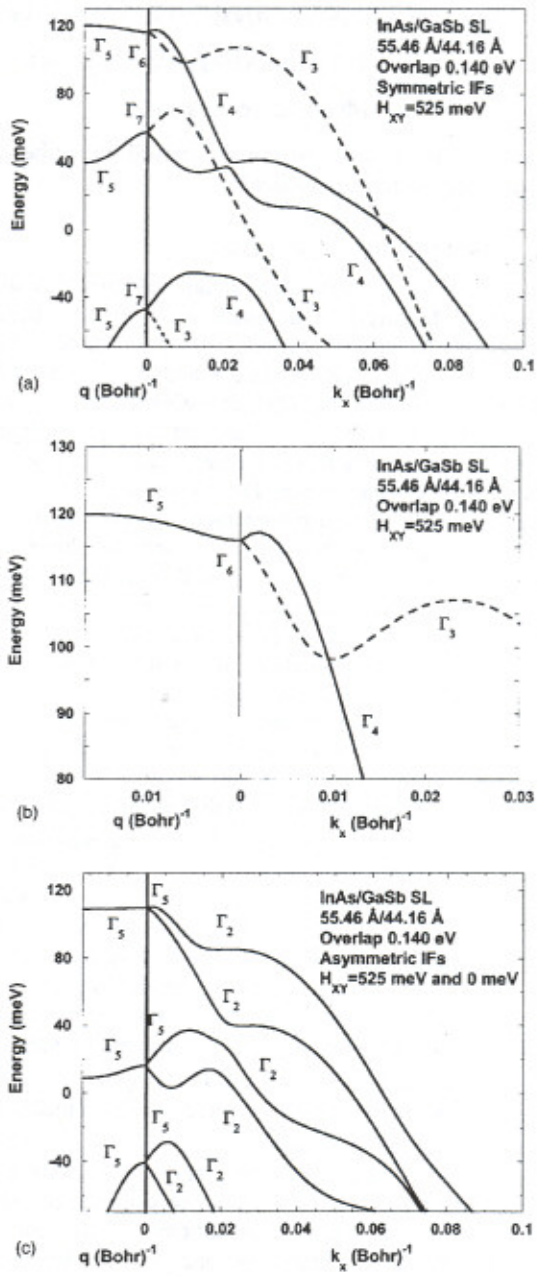

FIG. 2. The energy band structure for the test superlattice using the modified 8×8 EFA model based on the solution of the boundary value problem, Eqs. (21) or (22). Along the [100] direction, the bands are spin split. In the [001] direction, the bands remain doubly degenerate. From top to bottom, the bands derive from HH1, LH1, and HH2 bands in Fig. 1 and are strongly intermixed. The irreducible representations are labeled for the given directions using the notation from G. F. Koster, J. O. Dimmock, R. G. Wheeler, and H. Statz, *Properties of the Thirty Two Point Groups* (MIT Press, Cambridge, 1963). (a) Symmetric SL (point group D_{2d}) characterized by $H_{XY}=525$ meV or $t=5.12$ for both IF's; spin-split bands belong to different representations. (b) Valence band detail for the symmetric SL. (c) Asymmetric SL (point group C_{2v}) characterized by $H_{XY}=525$ meV for one IF and $H_{XY}=0$ meV for the other; spin-split bands belong to the same representation.

TABLE I. The first few bands (in meV) of the test SL at $\bar{\Gamma}$ as a function of the number of bands included in the $\mathbf{k}\cdot\mathbf{P}$ perturbative solution. The second column gives 6 of 15 bands used as input to the $\mathbf{k}\cdot\mathbf{P}$ perturbation expansion.

Band	8×8 EFA Input	3 Bands $\mathbf{k}\cdot\mathbf{P}$	5 Bands $\mathbf{k}\cdot\mathbf{P}$	6 Bands $\mathbf{k}\cdot\mathbf{P}$	7 Bands $\mathbf{k}\cdot\mathbf{P}$	10 Bands $\mathbf{k}\cdot\mathbf{P}$	13 Bands $\mathbf{k}\cdot\mathbf{P}$	14 Bands $\mathbf{k}\cdot\mathbf{P}$
LH3	−435.46			−441.06	−441.06	−399.57	−395.01	−395.27
LH2	−336.08			−399.75	−399.57	−384.63	−383.80	−382.80
HH3	−253.93		−255.19	−193.50	−193.49	−193.49	−190.30	−191.30
HH2	−40.32		−67.13	−64.44	−64.44	−55.97	−55.73	−55.73
LH1	−31.96	−31.96	−5.15	−3.25	−3.25	10.43	10.92	10.92
HH1	94.53	93.76	93.77	97.77	97.77	97.77	98.17	97.28

(c) At $\bar{L}$, HH1 is antisymmetric about the center of InSb layer and LH2 is symmetric about the center of GaSb layer, so that the HH1-LH2 integral V_{12} is again nonzero. HH1 band is shifted upward, and the HH1 band acquires the negative curvature of the LH2 band at $\bar{L}$ [compare Fig. 1 to Fig. 2(a)].

(d) On general grounds, anisotropic IF interactions force the band gap to be indirect, with the valence band maximum being either close to $\bar{\Gamma}$ or at $\bar{L}$. This effect can be tested by examining absorption tails.

(e) For an asymmetric SL of Fig. 2(c), one of the IF's does not contribute to the interaction matrix so that the size of effects seen in Fig. 2(a) is reduced. In the limit of equal and opposite H_{XY} at the IF's, HH1 interacts with LH1, not LH2.

(f) Using the same perturbative calculation, the shift of HH1 due to its interaction with SO2 (second spin-orbit band) is proportional to t^2/Δ.

G. Comparison to perturbative k·P solutions

Paralleling the calculation of Ref. 30, the problem was also solved perturbatively by first order perturbation theory, with Eq. (4) as the perturbation. Inputs to this calculation are the 8×8 EFA envelope functions at $\bar{\Gamma}$,

$$F_v^N(\mathbf{k}_\parallel=0,q=0,z)=\sum_{i=1}^{2N} C_v(\mathbf{k}_\parallel=0,k_i)\exp(ik_iz) \times c_i^N(\mathbf{k}_\parallel=0,q=0) \tag{39}$$

and energies $E_N(\mathbf{k}_\parallel=0,q=0)$ for band N from the standard 8×8 EFA. Using the wave function expansion in layer B (here, InAs), the first order perturbation matrix between bands N and M is given by

$$V_{NM}=a_0\sum_{\substack{i,j\\ v,\mu}} C_v(k_i)^*C_\mu(k_j)(\beta_i^N)^*\beta_j^M\{(H_{XY}^{AB}+H_{XY}^{BA}) \times\Theta_{v\mu}(1+i\tan k_jb\tan k_i^*b)+i(H_{XY}^{AB}-H_{XY}^{BA}) \times\Theta_{v\mu}(\tan k_jb-\tan k_i^*b)\}, \tag{40}$$

where

$$\beta=(\cos K_Bb)c_B. \tag{41}$$

To first order, the perturbation matrix depends on the sum and difference of the perturbing IF terms.

The perturbative solution was tested as a function of the number of bands included in the perturbative treatment, Table I. Using the test SL with symmetric IF's, up to 15 bands were calculated at $\bar{\Gamma}$, including $C1$ through $C2$, HH1 through HH7, and LH1 through LH6, spanning the interval from about −700 to 600 meV. The size of the perturbation matrix elements $|V_{NM}|^2/(E_M-E_N)$ converged rapidly, implying that the degenerate perturbation theory should also be convergent.

From Table I, about 14 (28 with spin) bands are required to converge the first few bands. The HH1 band shifts by only 3 meV as the result of interaction with 14 bands, indicating weak coupling. The LH1 band is greatly affected, moving by

TABLE II. First few energy levels for the test SL with symmetric IF's characterized by $H_{XY}=525$ meV calculated via the 14×14 perturbative $\mathbf{k}\cdot\mathbf{P}$ scheme, Eq. (40), and with the present BC approach, Eq. (29). Separate columns are for results without IF coupling to the SO or LH bands.

Level	$H_{XY}=0$ 8×8 EFA	$\mathbf{k}\cdot\mathbf{P}$ No SO	$\mathbf{k}\cdot\mathbf{P}$ No LH	$\mathbf{k}\cdot\mathbf{P}$ All	BC No SO	BC No LH	BC All
$C1$	205.92	212.54	207.18	208.18	216.55	208.36	212.23
HH1	94.53	93.42	94.64	97.28	93.47	100.54	115.96
LH1	−31.96	−4.84	−27.01	10.92	−3.91	−13.09	57.32
HH2	−40.32	−58.80	−35.87	−55.73	−58.68	−33.16	−47.64
HH3	−253.93	−228.19	−238.33	−191.30	−224.24	−192.40	−102.28
LH2	−336.08	−362.84	−352.18	−383.80	−355.51	−345.02	−367.85

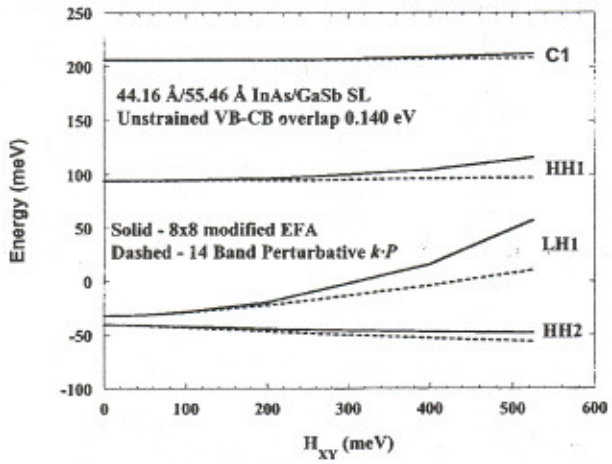

FIG. 3. Plots of the C1, HH1, LH1, and HH2 eigenvalues for the perturbative 14×14 **k**·**P**, Eq. (41), and the modified 8×8 EFA, Eq. (21), approaches as a function of the strength of the IF interaction for the test superlattice.

some 40 meV, since symmetric IF's couple opposite parity LH-HH pairs such as LH1 and HH2. Similarly, HH1 and LH2 bands are expected to interact, but for the parameters of the test SL, these bands are already separated by 450 meV. The symmetric IF's have almost no effect on the conduction band (not shown in Table I).

Table II provides a comparison of the calculated energy levels for the test SL, Figs. 1 and 2, using the 14×14 perturbative **k**·**P** solution and the BC method with the modified 8×8 EFA. For the perturbative solution, we use 14 doubly degenerate bands calculated at $\bar{\Gamma}$—one conduction band and thirteen valence bands. One finds that as long as the SO band is not included (both "no SO" columns), the results of the perturbative **k**·**P** and the BC methods are comparable, although the BC approach gives slightly more positive energies especially for the deeper bands for which the **k**·**P** approach is less converged. There are much greater differences between the **k**·**P** and BC methods in the "no L" columns, where only the HH-SO IF coupling is retained. With all interactions included, the differences between the **k**·**P** and BC columns are very large. We contend that the perturbative **k**·**P** method cannot adequately represent the IF-peaked SO wave function, whose large curvature adds more kinetic energy to energy eigenvalues than is reflected in the **k**·**P** approach.

Figure 3 plots $C1$, HH1, LH1, and HH2 eigenvalues in the 14×14 **k**·**P** and 8×8 BC approaches as a function of the strength of the IF interaction. HH1 rises in energy with increasing interaction strength as the result of its hybridization with lower bands. The greatest difference between the two calculations is for the LH1 level because it contains the largest SO admixture due to the direct LH-SO coupling in the **k**·**p** Hamiltonian. The HH1 difference is 22 meV, which although small on the scale of the graph (or on the scale of the VB offset, i.e., depth of the VB QW), is very large on the scale of the band gap of 100 meV. The large difference in the LH1 energies would result in greatly different Auger lifetimes predicted by the two calculations based on exactly the same Hamiltonian. Lastly, calculated interband absorption peaks in the BC approach would be closer spaced than in the **k**·**P** approach.

Another way of studying the influence of the spin-orbit band is to consider Table III, which breaks down various components of the calculation. Without IF coupling, $H_{XY}=0$, in going from the 4×4 to 6×6 and then 8×8 EFA results, the very large effect of the **k**·**p** coupling of the LH1 band to the SO and C bands is apparent. With the full interaction turned on, the 14×14 model gives lower energies, as noted in Fig. 3. By comparing the three **k**·**P** calculations, it is clear that the full effect of the IF interaction is turned on only when the SO band is included. With HH-LH IF coupling only, the positions of the three (and most other) bands in the BC 8×8 EFA and the 14×14 **k**·**P** perturbation model are very similar, indicating the crucial importance of the IF coupling to the SO band.

TABLE III. The calculated energies (in meV) for the test SL at $\bar{\Gamma}$ using several models for the modified EFA (BC columns) and the 14×14 perturbative **k**·**P**.

Interaction	Level	4×4 HI BC	6×6 HLS BC	8×8 CHLS BC	14×14 **k**·**P** Perturbative
$H_{XY}=0$	HH1	94.53	94.53	94.53	94.53
	LH1	−29.54	−10.75	−31.96	−31.96
	HH2	−40.32	−40.32	−40.32	−40.32
$H_{XY}=252$ meV	HH1	96.76	120.66	115.96	97.28
All	LH1	8.85	69.62	57.32	10.92
	HH2	−64.46	−36.76	−47.65	−55.73
$H_{XY}=525$ meV	HH1	96.76	97.98	93.48	93.42
HH-LH IF	LH1	8.85	22.74	−3.91	−4.83
Coupling	HH2	−64.46	−55.45	−58.68	−58.80
$H_{XY}=525$ meV	HH1		102.49	100.54	94.64
HH-SO IF	LH1		−8.71	−13.09	−27.01
Coupling	HH2		−11.66	−33.16	−35.87

Lastly, Table III shows that the effects of the HH-LH and HH-SO IF couplings are not simply additive—the problem is highly nonlinear. An additional reason for studying the 4 $\times$4 and 6$\times$6 models here is that they are devoid of possible spurious solutions that sometimes appear in the 8$\times$8 EFA model.

The BC approach solves the problem exactly and should be used as the standard of comparison. The BC method is "horizontal"—each wave function is expanded in terms of properly joined solutions of the bulk problem at the energy and wave vector of interest, Eq. (6). The perturbation approach is "vertical"—each wave function is expanded in terms of the eigenstates of the unperturbed Hamiltonian (39) that are ascending in energy. For example, in the BC method, the wave function of the HH1 state has SO components at the energy of the HH1 state, components that are very sharply peaked at the IF's, since the SO state is highly evanescent at the energy of the HH1 state. Already in the tight-binding calculation of Schulman and Chang[7] (see their Table VI), HH states are shown to have large LH and SO admixtures at $\bar{\Gamma}$.

Additionally, in Appendix E, a test case demonstrates that HH1 in a model SL shifts more when computed in the 6 $\times$6 HLS model than in the 4$\times$4 HS and 4$\times$4 HL models combined. This implies that the problem is highly nonlinear, thus inappropriate for perturbative treatment. Then, in Appendix F, we prove that the anisotropic interaction at a single IF is so singular that it can bind a hole.

Overall, the present results indicate that the spin-orbit band is very important both qualitatively and quantitatively. In particular, the position of the HH1 valence band is seen to vary greatly when the IF coupling to the SO band is included. Already, Ivchenko, Kaminski, and Rössler[42] showed that the SO band is important in fitting the anisotropic exchange splitting of excitonic levels in GaAs/AlAs SL's by demonstrating that the fit changes from $t=1.4$ to $t=0.5$ without and with the SO band included, respectively.[42]

IV. COMPARISON TO EXPERIMENT

In order to compare experiment to theory, the modified EFA requires H_{XY} parameters for the GaAs-like and InSb-like IF's. For a symmetric structure, however, only one H_{XY} parameter is required. For the determination of this parameter, we grew and measured the photoresponse of two sets of InAs/GaSb SL's with InSb IF's—one with variable GaSb layer widths and the other with variable InAs layer widths.[56]

A. Experimental

The InAs/GaSb SL's were grown by molecular beam epitaxy (MBE) using elemental metals for Ga, In, and valved cracker cells for Sb and As. The substrates were epiready (100) Te-doped GaSb wafers. First, GaSb buffer layers were grown on the substrates at the growth temperature of 480 °C. Next, the temperature was lowered to 410$\pm$5 °C to grow the SL structure. Here, growth temperatures are pyrometer readings referenced to the GaSb oxide desorption temperature of 530 °C. The InSb-like IF bonds were inserted between the layers to reduce the SL strain. The number of SL periods was fixed at 40 and the growth rates of GaSb, InAs, and InSb were 1.32, 0.38, 0.47 Å/s, respectively. The samples in the same series were grown consecutively within a short time period to minimize the variation of growth rates. The shutter sequence process within the series was kept the same to ensure consistent intermixing between the layers. The V/III beam equivalent pressure flux ratio was approximately 3.5 for the InAs and 2.5 for the GaSb growth. Cracker temperatures were 900 °C for As and 850 °C for Sb. These growth conditions were optimized for the smoothest surface morphology and the best structural quality. With optimized conditions, the MBE growth process maintained the intended period within 1 Å.

TABLE IV. The positions of the first heavy hole (HH1) and conduction ($C1$) bands for two values of unstrained InAs conduction/GaSb valence band overlaps

InAs/GaSb Overlap (eV)	InAs (Å)	GaSb (Å)	HH1 (meV)	$C1$ (meV)
0.140	85	85	124.95	129.99
	86	86	125.26	127.94
	87	87	125.85	123.96
0.150	83	83	134.17	135.83
	84	84	134.69	133.71
	85	85	134.92	131.61

To determine the actual SL period and strain, high-resolution x-ray rocking curve (HRXRD) measurements were performed. The actual periods were determined from the SL satellite peak splitting in the (004) spectra. For the present study, individual layer thicknesses were only estimated but are expected to be close to the nominal values. It is reasonable to assume that the precisely calibrated growth rates and a consistent shutter sequence process within the series should provide highly accurate individual layer thicknesses with consistent intermixing between the layers.

To determine the band gap energies and other band structure parameters, Fourier transform infrared (FTIR) photoresponse spectroscopy was used. The spectral response for this series was measured using a BIO-RAD 6000 FTIR spectrometer system. The samples were contacted with indium stripes and then illuminated from the front at normal incidence. The spectra were collected at 10 K.

B. Fitting VB-CB overlap

The EFA requires a few parameters to be fixed by experimental data. For individual layers, the required data comes from measurements on the constituent bulk components of the SL, Table IX, Appendix D. This leaves only information on the IF's, among them the conduction-valence band overlap. While this offset has been measured by independent experiments and calculated theoretically, here the offset is fixed by using the fact that for equal width SL's, the metal-insulator transition takes place at about 83.5Å,[64] at which anisotropic IF effects are negligible. Table IV shows that the VB-CB overlap of 0.150 eV gives the best fit to the S-M

TABLE V. Band extrema and the conduction band bandwidth for a series of grown SL's with the InAs width of 20.5 Å and the GaSb width ranging from 18 to 27 Å and purposefully grown InSb IF's. The unstrained VB-CB overlap of 150 meV was used.

GaSb width (Å)	HH1 (meV)	$C1$ $\overline{\Gamma}\rightarrow\overline{L}$	E_g (meV)	Exp. (meV)	Bandwith $\overline{L}-\overline{\Gamma}$	Centroid $(\overline{L}+\overline{\Gamma})/2$
27	131.6	438.1→626.1	306.5	299	187.9	532.1
24	129.3	421.8→641.9	292.5	293	220.1	531.2
21	126.4	402.3→660.8	276.1	279	258.5	531.5
18	121.8	378.7→683.3	256.9	254.5	304.6	531.0

transition point whereas the offsets of 0.140 produce the S-M transition around 86.5 Å. The 10 meV difference for the 1 ML difference in the layer widths gives an indication of the overall accuracy of the calculation.

C. Variable GaSb study

Four samples with GaSb widths ranging from 18 to 27 Å and the InAs width held constant at 20.5 Å were grown with InSb IF's as described above. The H_{XY} parameter characterizing InSb IF's was calculated by fitting the band gap of the 18 Å sample and then used in the calculations for the rest of the SL's in this paper. The value of $H_{XY}=580$ meV, or $t=5.66$, fit the gap to within a couple of meV. For comparison, Lau and Flatte[30] use symmetric and antisymmetric interaction potentials $V_S=500$ meV and $V_A=360$ meV, respectively, and Olesberg *et al.*[28] fit the spin relaxation times in short-period InAs/GaSb SL's with the V_A between 300 and 500. In another system, Ivchenko *et al.*[42] use $t=0.9$ and 0.32 for AlAs/GaAs and obtain a tight-binding estimate of $t=0.76$. Also, for an InAs/GaInP IF, Ivchenko, Toporov, and Voisin[44] find $t=-4.47$. Therefore, the present estimate is consistent with the order of magnitude found by others. The results for the other SL's in the series and the experimental band gaps are given in Table V.

The agreement between experiment and theory in Table V for the band gaps is very good, with small differences being within the uncertainties in the layer widths. The present modified 8×8 EFA calculation shows that heavy holes are largely confined in the GaSb layers while electron wave functions overlap considerably from one InAs layer to another. As GaSb layers become narrower, the HH-derived top of the valence band decreases in energy; at the same time, the overlap between the electron wave functions increases, leading to an increase in the CB bandwidth, Table V. With increasing CB bandwidth, the bottom of the CB decreases in energy at a rate greater than the decrease of the top of the VB, leading to the observed decrease in the band gap with decreasing GaSb layer width. Also, the center of the CB remains nearly constant, and only its top and bottom move, increasing the bandwidth. This trend is naturally explained in the tight-binding picture of band formation. The net effect is that the bottom of the CB moves down faster than does the HH band, thus the band gap narrows.

The fact that the CB rises/falls faster than the valence band with changes in GaSb thickness agrees with the findings of Ongstad *et al.*[22] We supplement these findings with our observation that the middle of the CB is largely invariant—only its bandwidth changes.

D. Variable InAs width study

Table VI presents the results of the variable InAs width study, with the InAs layer width ranging from 16 to 23.5 Å and the GaSb width held constant at 24 Å. The calculation uses the same asymmetry parameter $H_{XY}=580$ meV for both IF's as that used in Table V for the variable GaSb width study.

In Table VI, the HH1 level is largely invariant to InAs width variations, especially for thicker InAs layer widths. $C1$ varies in expected fashion, decreasing rapidly for larger InAs layer widths because of the small InAs CB mass. The experimental result for the 16 Å sample appears inconsistent with the results for the other four samples. The overall agreement is good with only one adjustable parameter obtained on a sample from a different set, Table V. The HH1-LH1 separation is much smaller than the gap so that Auger recombination cannot be suppressed through final state optimization.

TABLE VI. Calculated and measured band gaps for several InAs/GaSb SL's with a constant GaSb width of 24 Å and the InAs layer widths ranging from 16 to 23.5 Å. The same asymmetry parameter $H_{XY}=580$ meV as in Table V was used for both IF's. The unstrained VB-CB overlap of 150 meV was used.

InAs width (Å)	LH1 (meV)	HH1 (meV)	$C1$ (meV)	E_g (meV)	Exp. (meV)
16	74.34	132.67	503.20	370.53	343
17.5	70.37	130.99	477.67	346.68	340
19	66.69	129.71	454.05	324.34	314
20.5	63.26	128.73	432.16	303.43	298
23.5	58.05	127.36	392.93	265.57	269.6

E. 19 μm sample, Wei *et al.* (Ref. 11)

This sample—1 ML InSb IF's, 17 ML InAs, and 7 ML GaSb—was grown with both InSb IF's and is thus suitable for simulation using the previously found $H_{XY}=580$ meV. The results here are $C1=184.13$ meV and HH1 of 119.63 meV, for the gap of 64.5 meV, or a cutoff of 19.2 μm. The experimental numbers are 50% cutoff at 18.5 μm (66 meV) and a 0% cutoff of about 20.5 μm (or 60.5 meV). Also, LH1 = 25.48 meV, so HH1-LH1 separation is larger than the gap. The standard 8×8 EFA predicts a 7.5 μm cutoff.

F. 32 μm sample, Wei *et al.* (Ref. 12)

For this sample—1 ML InSb IF's 16 ML InAs, and 4 ML GaSb—we again use $H_{XY}=580$ meV and find $C1$ at 154.38 and HH1 at 102.43 for the gap of 51.95 meV. The experimental fit to R_0A (resistance-area product) data vs temperature for this sample yields the activation energy of 45.5 meV. The standard 8×8 EFA code[32] predicts a 5.5 μm cutoff. Overall, the results for SL's with controlled InSb IF's agree well with experiments both in the MWIR and LWIR windows for samples where IF effects should be large owing to the thinness of at least one of the layers.

G. Mixed interfaces

Ongstad *et al.*[22] and Kaspi *et al.*[23] grew two sets of samples with mixed IF's. Using $H_{XY}=580$ meV for InSb-like IF's, we use the band gap of the 6 ML/6 ML sample to fit the coupling parameter for GaAs-like IF's. If one were to fit both parameters at the same time, the graph of H_{XY}^{InSb} vs H_{XY}^{GaAs} would yield an oval curve, thus the need to fix one of the parameters beforehand. Even with one H_{XY} fixed, the calculated band gaps are a rapidly varying function of the other H_{XY}.

Table VII presents the experimental-theoretical comparison for the mixed-IF samples where the InAs width is held constant at 6 ML. The measured band gap for the 6 ML/6 ML SL was well fit with $H_{XY}^{\mathrm{GaAs}}=0$ meV and H_{XY}^{InSb} held fixed at 580 meV. This does not mean that GaAs IF's do not introduce a perturbation, only that reasonably good fits can be obtained for H_{XY} around zero to within the accuracy of the calculation since a small variation of H_{XY}^{InSb} can lead to a large variation of H_{XY}^{GaAs} (e.g., Fig. 3). In addition, we have no direct comparison between the IF's grown by Ongstad *et al.* and Kaspi *et al.* and those grown in our lab. The small value of H_{XY}^{GaAs} indicates that IF effects for mixed interface SL's are smaller that for SL's with both InSb-like IF's.

Next, Table VIII presents the experimental-theoretical comparison for the mixed-IF samples of Kaspi *et al.*, where the InAs width is held constant at 8 ML and the theoretical IF parameters are held at $H_{XY}^{\mathrm{InSb}}=580$ meV and $H_{XY}^{\mathrm{GaAs}}=0$ meV as in Table VII. The true valence band maximum for the cases of Tables VII and VIII is slightly away from the zone center and not more than 0.5 meV greater than the center zone values listed in the tables. In both tables, the agreement with experiment is very good and comparable to that found in the SEPM (Ref. 22) and EPM calculations.[17] The results of variable GaSb width studies in Tables V, VII, and VIII are presented in Fig. 4.

TABLE VII. Experimental-theoretical comparison for the mixed-IF series with the a 6 ML InAs. Here $H_{XY}=580$ meV for the InSb IF and $H_{XY}=0$ meV for the GaAs IF. Unstrained InAs CB/GaSb VB overlap of 0.150 eV. The band gap data are from Refs. 22 and 23.

ML's	InAs	GaSb	HH1 (meV)	$C1$ (meV)	E_g (meV)	Exp (meV)
6/6	18.18	18.29	103.78	418.75	315.1	318 PL 326 Abs
6/9	18.18	27.43	121.74	487.10	365.4	355 PL 358 Abs
6/12	18.18	36.57	130.59	527.06	396.5	382 PL 386 Abs
6/18	18.18	54.56	138.81	566.66	427.9	415 PL 416 Abs
6/24	18.18	73.14	142.65	583.31	440.7	425 PL 427 Abs

V. CONCLUSIONS

The band structure of InAs/GaSb SL's was investigated within the framework of the 8×8 EFA method, modified by the inclusion of IF effects, based on the solution of the associated boundary-value problem and the Ivchenko-Kaminski-Rössler representation of the IF Hamiltonian. It was found that a consistent application of the theory requires the inclusion of the SO band and that its inclusion dramatically alters the bands from those calculated with the HH-LH IF coupling alone. With the inclusion of the H-SO IF coupling, perturbative solutions converge to incorrect limits because the SO admixture is highly peaked at the IF's and the IF interaction is singular enough to potentially bind a hole at the IF.

For a test InAs/GaSb SL with symmetric IF's and for reasonable strengths of the IF interaction, the band structure exhibited large splittings and avoided crossings. Analytic solution of the EFA model in several important limits provided additional physical insight into the band formation in SL's and QW's in the presence of IF effects. The calculated results were also verified against these analytical models.

Very good agreement was found between experimental results and theory on several sets of SL's (both MWIR and LWIR) with symmetric InSb IF's, using one adjustable pa-

TABLE VIII. Same as Table VII for the mixed-IF series with the InAs layer width of 8 ML.

ML's	InAs	GaSb	HH1 (meV)	C1 (meV)	E_g (meV)	Exp (meV)
			111.74	385.07	273.33	277 PL
8/8	24.23	24.38				
						283 Abs
			127.04	437.69	310.65	304 PL
12/8	24.23	36.57				
						308 Abs
			134.38	464.70	330.32	330 PL
16/8	24.23	48.76				
						332 Abs
			141.17	486.92	345.75	346 PL
24/8	24.23	73.14				
						351 Abs
			144.20	493.56	339.36	346 PL
32/8	24.23	97.53				
						350 Abs
			145.86	495.57	349.7	352 PL
40/8	24.23	121.91				
						353 Abs

rameter for the strength of the IF interaction at InSb-like IF's. Then, with one more adjustable parameter for GaAs IF's, very good agreement was found for two series of samples with mixed GaAs-like and InSb-like IF's.

Overall, it was shown that a consistent application of the EFA method with the inclusion of well established IF effects can provide useful physical insights and possesses good predictive capacity in the design of NCA SL's. The formalism derived here is algorithmically simple, numerically stable, computationally fast, and capable of providing rich physical insight into band formation in SL's.

ACKNOWLEDGMENTS

The authors would like to thank Eduard Takhtamirov, Ph.D., Senior Scientist, Institute of Radioengineering and Electronics of RAS, Moscow, Russia, and Professor Voisin for useful communications. The work of F.S. was supported by the Air Force Contract No. F33615-00-C-5422 at the Materials Lab, AFRL/ML.

APPENDIX A: INTERFACE MATRIX

The $2N\times 2N$ interface matrix [Eq. (14)] was defined as

$$\Phi = H_{XY} a_0 \begin{pmatrix} 0 & 0 \\ \Theta & 0 \end{pmatrix}, \tag{A1}$$

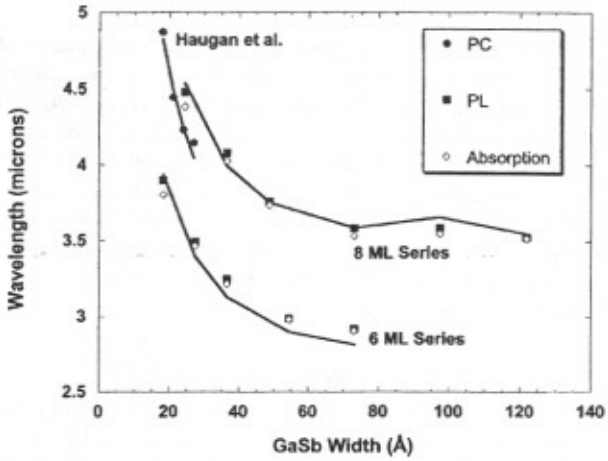

FIG. 4. Collected results of the variable GaSb width studies listed in Tables V, VII, and VIII, where the solid curves are calculated with the modified EFA and the experimental data are from Haugan *et al.* (Ref. 56), Ongstad *et al.* (Ref. 21), and Kaspi *et al.* (Ref. 23).

where the $N\times N$ matrix Θ is Hermitian. Matrix Φ cannot be diagonalized by a similarity transformation but, nevertheless, has several interesting properties.

(1) Multiplicative inverse

$$(I - i\Phi) = \begin{pmatrix} I & 0 \\ -iH_{XY}a_0\Theta & I \end{pmatrix} = (I + i\Phi)^{-1}. \tag{A2}$$

(2) Multiplicative associativity

$$(I + i\Phi_1)(I + i\Phi_2) = [I + i(\Phi_i + \Phi_2)]. \tag{A3}$$

All these properties are shared with the exponential matrix defined through the Taylor expansion

$$\exp(i\Phi) \equiv I + i\Phi + (i\Phi)^2/2 + \cdots = I + i\Phi, \tag{A4}$$

since all powers of Φ, Eq. (A1), higher than the first are zero. Analogously to Eqs. (A2) and (A3), it follows that

$$\exp(-i\Phi) = [\exp(i\Phi)]^{-1}, \tag{A5}$$

$$\exp(i\Phi_1)\exp(i\Phi_2) = \exp[i(\Phi_1 + \Phi_2)]. \tag{A6}$$

Also, the determinant

$$\|\exp(i\Phi)\| = 1. \tag{A7}$$

Moreover, trigonometric functions defined through the exponential satisfy

$$\sin\Phi = \tan\Phi = \begin{pmatrix} 0 & 0 \\ \Phi & 0 \end{pmatrix}, \tag{A8}$$

$$\cos\Phi = I, \tag{A9}$$

and such identities as

$$\sin^2\Phi + \cos^2\Phi = I, \quad \sin 2\Phi = 2\sin\Phi\cos\Phi,$$

$$\cos 2\Phi = I - 2\sin^2\Phi,$$

$$\tan(\Phi/2) = \sin\Phi/(I+\cos\Phi),$$

and others not involving inverses of sines or tangents (i.e., cotangents or cosecants) because Eq. (A8) is not invertible.

However, the exponential matrix lacks one important property—it is not diagonalizable via a similarity transformation, the usual method for evaluating the exponential of a matrix. Here, the exponential is evaluated from its series expansion (A4), which has only two terms. Moreover, the argument of the exponential is not dimensionless, so that it must be understood that the exponential acts on column vectors of the form $(F,F')^T$, where the lower half is the spatial derivative of the upper half. With these provisos, the use of Eq. (A4) in the development following Eq. (13) is internally consistent and achieves notational simplicity and transparency.

APPENDIX B: TRANSFER MATRIX METHOD

The EFA boundary conditions require the continuity of

$$\begin{pmatrix} I & 0 \\ H_1/2 & H_2 \end{pmatrix}\begin{pmatrix} iF \\ F' \end{pmatrix} \equiv Sf \tag{B1}$$

across all interfaces (e.g., $S_A f_A = S_B f_B$), where

$$f = \begin{pmatrix} iF \\ F' \end{pmatrix}, \tag{B2}$$

unless there is a delta function discontinuity in the Hamiltonian at an interface, e.g., $H_{XY} a_0 \delta(z)\Theta$, in which case an additional phase factor comes in. For example, in crossing the BA interface, the continuity equation reads

$$S_B f_B = \exp(i\Phi_{BA}) S_A f_A, \tag{B3}$$

where

$$\exp(i\Phi_{BA}) = \begin{pmatrix} I & 0 \\ iH_{XY}a_0\Theta & I \end{pmatrix}.$$

Also, at AB IF, $S_A f_A = \exp(-i\Phi_{AB}) S_B f_B$.

The second-order Schrödinger equation is changed into the first-order equation

$$i\Omega(z) f(z) = \frac{df(z)}{dz}, \tag{B4}$$

where Ω is the $2N \times 2N$ matrix

$$i\Omega = \begin{pmatrix} 0 & I \\ -H_2^{-1}(H_0 - E) & -H_2^{-1}H_1 \end{pmatrix}. \tag{B5}$$

In regions of constant composition, Ω is constant, so that the formal solution of Eq. (B4) is[32,62]

$$f(z) = \exp(i\Omega z) f(0) \equiv T(z) f(0), \tag{B6}$$

where $f(0)$ is a constant of integration and $T(z) \equiv \exp(i\Omega z)$ is the transfer matrix. If P diagonalizes Ω,

$$P^{-1}\Omega P = K, \tag{B7}$$

where K is diagonal, $K_{ij} = k_i \delta_{ij}$, $i = 1,\ldots,2N$, which defines a set of exponents $\{k\}$, then

$$\exp(i\Omega z) = P \exp(iKz) P^{-1}, \tag{B8}$$

where

$$[\exp(iKz)]_{ij} = \exp(ik_i z)\,\delta_{ij}. \tag{B9}$$

Integrating Eq. (B4) across one period from $-b$ to $b + 2a$, one finds

$$\begin{aligned} f_A(2a+b) &= \exp(i2\Omega_A a) f_A(b) = \exp(i2\Omega_A a) \\ &\times S_A^{-1} \exp(-i\Phi_{BA}) S_B \exp(i2\Omega_B b) f_B(-b) \\ &= \exp(i2\Omega_A a) S_A^{-1} \exp(-i\Phi_{BA}) S_B \exp(i2\Omega_B b) \\ &\times [S_B^{-1} \exp(i\Phi_{AB}) S_A f_A(-b)], \end{aligned} \tag{B10}$$

where $f_{A,B}$, $S_{A,B}$ stand for quantities evaluated at the A, B side of a particular interface; in Eq. (B10), two interfaces have been crossed. Next, employing the Bloch's theorem

$$f_A(2a+b) = \exp(iqd) f_A(-b) \tag{B11}$$

leads the secular equation

$$\begin{aligned} &\{[S_A \exp(i2\Omega_A a) S_A^{-1}] \exp(-i\Phi_{BA}) \\ &\times [S_B \exp(i2\Omega_B b) S_B^{-1}] \exp(i\Phi_{AB}) - \exp(iqd)\} \\ &\times f_A(-b) = 0. \end{aligned} \tag{B12}$$

Define matrix M [same as Eq. (12) in the text] as

$$\begin{aligned} S \exp(i\Omega z) S^{-1} &= (SP) \exp(iKz) (SP)^{-1} \\ &\equiv M \exp(iKz) M^{-1}, \end{aligned} \tag{B13}$$

where

$$M \equiv SP. \tag{B14}$$

Next, Eq. (B14) can be used to define the final exponential matrix

$$\exp(i\Lambda z) \equiv M \exp(iKz) M^{-1}, \tag{B15}$$

so that the secular equation (B12) becomes

$$\begin{aligned} &[\exp(i2\Lambda_A a) \exp(-i\Phi_{BA}) \exp(i2\Lambda_B b) \exp(i\Phi_{AB}) \\ &- \exp(iqd)] f_A(-b) = 0, \end{aligned} \tag{B16}$$

in which the unknowns are energy and vector $f_A(-b)$. Equation (B16) can be shown to be the same as the Eq. (16) in the text and can be used to derive the Kronig-Penney form, Eq. (30). Clearly, the transfer matrix derivation can be generalized to any number of layers per superlattice period.

APPENDIX C: ANALYTIC MODELS

1. IF coupling of HH and LH bands at $\bar{\Gamma}$

For the coupling of the HH and LH bands, the 4×4 problem at $\bar{\Gamma}$ decouples into two identical 2×2 EFA problems, so that all bands remain doubly degenerate. Consider then the 2×2 EFA case for the coupling of otherwise uncoupled parabolic HH and LH bands in Eq. (29). For parabolic bands[32]

$$\tan \Lambda_A a = \begin{pmatrix} 0 & 0 & 2A_H m_H/\hbar^2 k_H & 0 \\ 0 & 0 & 0 & 2A_L m_L/\hbar^2 k_L \\ \hbar^2 k_H A_H/2m_H & 0 & 0 & 0 \\ 0 & \hbar^2 k_L A_L/2m_L & 0 & 0 \end{pmatrix}, \tag{C1}$$

where $A_{H,L}=\tan k^A_{H,L}a$, $k^A_{H,L}=\sqrt{2m^A_{H,L}(E-V_0)/\hbar^2}$, and V_0 is the valence band offset. A similar equation for $\tan \Lambda_B b$ has $B_{H,L}=\tan k^B_{H,L}b$, $k^B_{H,L}=\sqrt{2m^B_{H,L}E/\hbar^2}$. For symmetric interfaces, the interface matrix is given by

$$\exp(i\Phi)=\begin{pmatrix} 1 & 0 & 0 & 0 \\ 0 & 1 & 0 & 0 \\ 0 & -T & 1 & 0 \\ T & 0 & 0 & 1 \end{pmatrix}, \tag{C2}$$

where

$$T=\frac{1}{\sqrt{3}}\left(\frac{\hbar^2 t}{2m_0 a_0}\right). \tag{C3}$$

Altogether, Eq. (29) for a symmetric SL at $\bar{\Gamma}$ can be solved to yield the following product of two determinants:

$$[A_H m^A_H/k^A_H + B_H m^B_H/k^B_H][k^A_L A_L/m^A_L + k^B_L B_L/m^B_L + (2T/\hbar^2)^2 A_H m^A_H/k^A_H] - (2T/\hbar^2)^2 (A_H m^A_H/k^A_H)^2 = 0 \tag{C4}$$

and

$$[A_L m^A_L/k^A_L + B_L m^B_L/k^B_L][k^A_H A_H/m^A_H + k^B_H B_H/m^B_H + (2T/\hbar^2)^2 A_L m^A_L/k^A_L] - (2T/\hbar^2)^2 (A_L m^A_L/k^A_L)^2 = 0 \tag{C5}$$

that are independent of the sign of T and are real, an important check on numerical results.

For simplicity, also let $m_{H,L}$ be continuous across interfaces. Then, in the limit of a quantum well ($a\to\infty$), $k_{H,L}A_{H,L}\to -\kappa_{H,L}$, where $\kappa_{H,L}=\sqrt{2m_{H,L}(V_0-E)/\hbar^2}$. Then, Eq. (C4) becomes

$$(\kappa_H + k_H \cot k_H b)(\kappa_L - k_L \tan k_L b) - (2T/\hbar^2)^2 (m_H m_L) = 0. \tag{C6}$$

Here, the first and the second factors are recognized as the conditions for odd HH and even LH bound states, respectively, in the limit of no LH coupling. Therefore, the coupling connects states such as HH2 and LH1.

The second solution yields

$$(k_L \cot k_L b + \kappa_L)(k_H \tan k_H b - \kappa_H) + (2T/\hbar^2)^2 (m_H m_L) = 0, \tag{C7}$$

which couples odd LH and even HH states, e.g., HH1 and LH2. This equation is identical to that derived by Ivchenko, Kaminskii, and Aleiner.[46]

The equations coupling the other two states $|\frac{3}{2},-\frac{3}{2}\rangle$ and $|\frac{3}{2},\frac{1}{2}\rangle$ are identical to the ones above, so that all bands are doubly degenerate at the center of the Brillouin zone. This is consistent with the symmetry analysis in Sec. III D for symmetric SL's.

2. Anisotropic HH-SO coupling at the center of the BZ

Similarly, for the coupling of the HH and SO bands, $|\frac{3}{2},\frac{3}{2}\rangle$ and $|\frac{1}{2},-\frac{1}{2}\rangle$, one finds

$$(\kappa_H + k_H \cot k_H b)(\kappa_S - k_S \tan k_S b) - 2(2T/\hbar^2)^2 (m_H m_S) = 0 \tag{C8}$$

and

$$(k_S \cot k_S b + \kappa_S)(k_H \tan k_H b - \kappa_H) + 2(2T/\hbar^2)^2 (m_H m_S) = 0, \tag{C9}$$

where $k_S=\sqrt{2m_S(E-\Delta)\hbar^2}$ and $\kappa_S = \sqrt{2m_S(\Delta+V_0-E)/\hbar^2}$. The factor of two shows that, all other things being equal, the HH-SO coupling is twice as strong as the HH-LH coupling.

3. Anisotropic HH-LH-SO coupling for a QW

A better indication of the combined effect of the HH-LH-SO coupling is found by solving a model of a QW with the coupling of $|\frac{3}{2},\frac{3}{2}\rangle$, $|\frac{3}{2},-\frac{1}{2}\rangle$, and $|\frac{1}{2},-\frac{1}{2}\rangle$. The Hamiltonian at the $z=b$ interface is given by

$$\begin{pmatrix} -\frac{\hbar^2}{2m_H}\frac{d^2}{dz^2} & iT\delta(z-b) & \sqrt{2}T\delta(z-b) \\ -iT\delta(z-b) & -\frac{\hbar^2}{2m_L}\frac{d^2}{dz^2} & -\frac{i\hbar^2}{2M}\frac{d^2}{dz^2} \\ \sqrt{2}T\delta(z-b) & -\frac{i\hbar^2}{2M}\frac{d^2}{dz^2} & -\frac{\hbar^2}{2m_S}\frac{d^2}{dz^2}+\Delta \end{pmatrix}\begin{pmatrix} F_H \\ F_L \\ F_S \end{pmatrix} = E\begin{pmatrix} F_H \\ F_L \\ F_S \end{pmatrix}, \tag{C10}$$

where, in terms of Luttinger parameters $m_0/m_H=\gamma_1-2\gamma_2$, $m_0/m_L=\gamma_1+2\gamma_2$, $m_0/m_S=\gamma_1$, and $m_0/M=2\sqrt{2}\gamma_2$. For symmetric interfaces, at $z=-b$, $T\to -T$.

In the limit of large spin-orbit energy, the envelope function for the symmetric state is given in the well by

$$\begin{pmatrix} F_H \\ F_L \\ F_S \end{pmatrix} = \begin{pmatrix} f_H \cos k_H z \\ f_L \sin k_L z - (im_L/M) f_S \sin k_S z \\ f_s \sin k_S z \end{pmatrix}, \quad |z| \le b, \tag{C11}$$

and in the right-hand barrier by

$$\begin{pmatrix} F_H \\ F_L \\ F_S \end{pmatrix} = \begin{pmatrix} (f_H \cos k_H b)\exp[-\kappa_H(z-b)] \\ (f_L \sin k_L b)\exp[-\kappa_L(z-b)] - (im_L/M) \\ \times (f_S \sin k_S b)\exp[-\kappa_S(z-b)] \\ (f_S \sin k_S b)\exp[-\kappa_S(z-b)] \end{pmatrix},$$

$$z > b, \tag{C12}$$

where the continuity of the envelope function at interfaces has been imposed. Here,

$$k_{H,L} = \sqrt{2m_{H,L}E/\hbar^2}, \quad k_S = i\sqrt{2\mu\Delta/\hbar^2},$$

$$\kappa_{H,L} = \sqrt{2m_{H,L}(V_0 - E)/\hbar^2},$$

$\kappa_S = \sqrt{2\mu(V_0+\Delta)/\hbar^2}$, and the "modified" spin-orbit mass is $1/\mu = 1/m_S - m_L/M^2$.

Integrating the Hamiltonian equation (C10) across an interface yields the secular equation

$$\frac{\hbar^2}{2m_H}(k_H \tan k_H b - \kappa_H) = -\frac{T^2}{\frac{\hbar^2}{2m_L}(k_L \cot k_L b + \kappa_L)} - \frac{2T^2(1 + M/\sqrt{2}m_L)^2}{\frac{\hbar^2}{2\mu}(\kappa_S + k_S \cot k_S b)}. \tag{C13}$$

Using the physical parameters of GaSb from Table IX, a comparison of the HH-SO model, Eq. (C9) with the HH-LH-SO model, Eq. (C13), shows that the effect of the SO band on the HH levels is enhanced by the factor

$$(1 + M/\sqrt{2}m_L)^2\sqrt{\mu/m_S} = 7.45 \tag{C14}$$

TABLE IX. Physical parameters used as input to the calculation (Ref. 63).

Parameter	Symbol	GaSb	InAs
Conduction band	E_C (meV)	Overlap+813.3	0
Valence band	E_V (meV)	Overlap	−410
Band gap	E_G (meV)	813.3	410
Momentum matrix	P^2 (eV)	25.84	22.04
Spin-orbit energy	Δ (meV)	752	380
Electron mass	m_C	$0.041\, m_0$	$0.023\, m_0$
Luttinger parameters	γ_1	11.8	19.67
	γ_2	4.03	8.37
	γ_3	5.26	9.29
Lattice constant	a_0 (Å)	6.0954	6.0584
Elastic constants	C_{11}	9.08×10^{11}	8.33×10^{11}
	C_{12}	4.13×10^{11}	4.53×10^{11}
	C_{44}	4.45×10^{11}	3.96×10^{11}
Deformation potentials (eV)	a_C	6.85	5.08
	a_V	0.79	1.00
	b_V	2.00	−1.8
	d_V	−4.8	3.6

by the LH-SO mixing. The present calculation was tested against the predictions of this Appendix using model QW's and SL's.

APPENDIX D: PHYSICAL PARAMETERS

APPENDIX E: LEVEL SHIFTS FOR VARIOUS COUPLINGS

The position of the HH1 level at $\bar{\Gamma}$ was examined using four modified EFA models, Table X. Clearly, the shift of the HH1 band does not depend linearly on the strength of the interface interaction, since the shift of the HH1 band in the LHS model is not the sum of the shifts in the HS and HL models even when weighted by the weights of the corresponding bands. In fact, the total shift is 11.4 meV, while the sum of unweighted shifts is 2.6+1.6=4.2 meV and of the weighted shifts is 17.6 meV. Observe that in a QW, there is a great density of bands above the top of the QW well, which must be taken into account in perturbative treatments that rely on the completeness of unperturbed solutions.

APPENDIX F: BOUND STATES OF THE IF POTENTIAL

Consider a hypothetical type-II alignment of two materials A and B with otherwise identical band parameters but whose interface, nevertheless, gives rise to a localized interface potential coupling parabolic HH and LH bands:

$$H = H_{\mathrm{EFA}} + H_{XY} a_0 \delta(z)\Theta, \tag{F1}$$

where H_{EFA} is the 4×4 $\mathbf{k}\cdot\mathbf{p}$ Hamiltonian for the heavy and light holes and H_{XY} is the Ivchenko-Kaminsky-Rössler interface coupling.

The EFA equation coupling $|\frac{3}{2}, \frac{3}{2}\rangle$ and $|\frac{3}{2}, -\frac{1}{2}\rangle$ manifolds becomes

$$\begin{pmatrix} -\frac{\hbar^2}{2m_H}\frac{d^2}{dz^2} & \frac{\hbar^2 t}{2m_0 a_0}\frac{i}{\sqrt{3}}\delta(z) \\ -\frac{\hbar^2 t}{2m_0 a_0}\frac{i}{\sqrt{3}}\delta(z) & -\frac{\hbar^2}{2m_L}\frac{d^2}{dz^2} \end{pmatrix} \begin{pmatrix} F_H \\ F_L \end{pmatrix} = E\begin{pmatrix} F_H \\ F_L \end{pmatrix}, \tag{F2}$$

TABLE X. The position of the HH1 level at $\bar{\Gamma}$ calculated using four modified EFA models with two symmetric IF's with $H_{XY}=525$ meV. In the 2×2 H model, the HH band is uncoupled; in the 4×4 HS model, the HH and SO bands are coupled by the IF's; in the 4×4 HL model, the HH and LH bands are coupled by the IF's; and in the 6×6 HLS model, the interface couplings are HH-SO and HH-LH, so that LH-SO interface coupling is indirect.

	HH1 (meV)	HH(%)	LH(%)	SO(%)
2×2 H	−50.78	100	0	0
4×4 HS	−48.20	99.86	0	0.14
4×4 HL	−49.17	99.79	0.21	0
6×6 HLS	−39.40	98.57	0.84	0.59

where the energy axis is up (effective masses are positive). Bound solutions are sought in the form

$$F_H = f_H \exp(-\kappa_H |z|)$$
$$F_L = f_L \exp(-\kappa_L |z|), \tag{F3}$$

where $\kappa_{H,L} = \sqrt{-2m_{H,L}E/\hbar^2}$ and the energy is negative. The eigenvalue equation has one doubly degenerate bound state at

$$E = -\left(\frac{\hbar^2 t}{2m_0 a_0}\right)^2 \frac{\sqrt{m_L m_H}}{2\hbar^2}$$

$$[\text{or } E = -(2.97 \text{ meV}) t^2 \text{ with GaSb parameters}]. \tag{F4}$$

Also, for a coupled H-SO system ($|\frac{3}{2}, \frac{3}{2}\rangle$ and $|\frac{1}{2}, -\frac{1}{2}\rangle$),

$$\begin{pmatrix} -\frac{\hbar^2}{2m_H}\frac{d^2}{dz^2} & \frac{\hbar^2 t}{2m_0 a_0}\sqrt{\frac{2}{3}}\delta(z) \\ \frac{\hbar^2 t}{2m_0 a_0}\sqrt{\frac{2}{3}}\delta(z) & -\frac{\hbar^2}{2m_{SO}}\frac{d^2}{dz^2} + \Delta \end{pmatrix} \begin{pmatrix} F_H \\ F_{SO} \end{pmatrix} = E \begin{pmatrix} F_H \\ F_{SO} \end{pmatrix}, \tag{F5}$$

which has one bound solution that, in the limit of large SO splitting, is given by

$$E = -\frac{m_H m_{SO}}{9\hbar^4 \Delta}\left(\frac{\hbar^2 t}{2m_0 a_0}\right)^4$$

$$[E = -(0.008 \text{ meV}) t^4 \text{ for GaSb}] \tag{F6}$$

and, in the limit of a large IF potential by

$$E = -\left(\frac{\hbar^2 t}{2m_0 a_0}\right)^2 \frac{\sqrt{m_H m_{SO}}}{3\hbar^2}$$

$$[E = -(2.58 \text{ meV}) t^2 \text{ for GaSb}]. \tag{F7}$$

Therefore, the IF potential by itself can bind a hole. For this reason, the problem is not amenable to perturbative treatments.

[1] D. L. Smith and C. Mailhiot, J. Appl. Phys. **62**, 2545 (1987); Surf. Sci. **196**, 683 (1988); Rev. Mod. Phys. **62**, 173 (1990).
[2] C. Mailhiot and D. L. Smith, J. Vac. Sci. Technol. A **7**, 445 (1989).
[3] G. J. Brown, F. Szmulowicz, K. Mahalingam, and S. Houston, Proc. SPIE **4999**, 457 (2003).
[4] J. R. Meyer, C. A. Hoffman, F. J. Bartoli, and L. R. Ram-Mohan, Appl. Phys. Lett. **67**, 757 (1995).
[5] Q. K. Yang, F. Fuchs, J. Schmitz, and W. Pletschen, Appl. Phys. Lett. **81**, 4757 (2002).
[6] J. N. Schulman and Y. C. Chang, J. Vac. Sci. Technol. B **1**, 644 (1983).
[7] J. N. Schulman and Y.-C. Chang, Phys. Rev. B **31**, 2056 (1980).
[8] J. R. Meyer (unpublished).
[9] F. Fuchs, E. Ahlswede, U. Weimar, W. Pletschen, J. Schmitz, M. Hartung, B. Jager, J. P. Kotthaus, and F. Szmulowicz, Appl. Phys. Lett. **73**, 3760 (1998).
[10] E. R. Heller, K. Fisher, F. Szmulowicz, and F. L. Madarasz, J. Appl. Phys. **77**, 5739 (1995); F. Szmulowicz, E. R. Heller, K. Fisher, and F. L. Madarasz, Superlattices Microstruct. **17**, 373 (1995).
[11] Y. Wei, A. Gin, M. Razeghi, and G. J. Brown, Appl. Phys. Lett. **80**, 3262 (2000).
[12] Y. Wei, A. Gin, M. Razeghi, and G. J. Brown, Appl. Phys. Lett. **81**, 3675 (2002).
[13] B. Jogai and D. N. Talwar, Phys. Rev. B **54**, 14 524 (1996); D. N. Talwar, John P. Loehr, and B. Jogai, *ibid.* **49**, 10 345 (1994).
[14] L.-W. Wang, S.-H. Wei, T. Mattila, A. Zunger, I. Vurgaftman, and J. R. Meyer, Phys. Rev. B **60**, 5590 (1999).
[15] R. Magri and A. Zunger, Phys. Rev. B **62**, 10 364 (2000).
[16] R. Magri and A. Zunger, Phys. Rev. B **64**, 081305 (2001).
[17] R. Magri and A. Zunger, J. Vac. Sci. Technol. B **21**, 1896 (2003); Phys. Rev. B **65**, 165302 (2002); **68**, 155329 (2003).
[18] R. Magri, J. W. Wang, A. Zunger, I. Vurgaftman, and J. R. Meyer, Phys. Rev. B **61**, 10 235 (2000).
[19] R. Magri and A. Zunger, Phys. Rev. B **62**, 10 364 (2000).
[20] M. R. Kitchin and M. Jaros, Physica E **18**, 498 (2003).
[21] M. R. Kitchin, J. P. Hagon, and M. Jaros, Semicond. Sci. Technol. **18**, 225 (2003).
[22] P. Ongstad, R. Kaspi, C. E. Moeller, M. L. Tilton, T. M. Gianardi, J. R. Chavez, and G. C. Dente, J. Appl. Phys. **89**, 2185 (2001).
[23] R. Kaspi, C. Moeller, A. Ongstad, M. L. Tilton, D. Gianardi, G. Denete, and P. Gopaladasu, Appl. Phys. Lett. **76**, 409 (2000).
[24] M. L. Tilton and G. C. Dente, J. Appl. Phys. **94**, 4705 (2003).
[25] G. C. Dente and M. L. Tilton, J. Appl. Phys. **86**, 1420 (1999).
[26] G. C. Dente and M. L. Tilton, Phys. Rev. B **66**, 165307 (2002).
[27] E. Corbin, M. J. Shaw, M. R. Kitchin, J. P. Hagon, and M. Jaros, Semicond. Sci. Technol. **16**, 263 (2001).
[28] J. T. Olesberg, W. H. Lau, M. R. Flatte, C. Yu, E. Altunkaya, E. M. Shaw, T. C. Hasenberg, and T. F. Boggess, Phys. Rev. B **64**, 201301 (2001).
[29] K. C. Hall, K. Gundogdu, E. Altunkaya, W. H. Lau, M. E. Flatte, T. Boggess, J. J. Zinck, W. B. Barvos-Carter, and L. Skeith, Phys. Rev. B **68**, 115311 (2003).
[30] W. H. Lau and M. E. Flatte, Appl. Phys. Lett. **80**, 1683 (2002).
[31] C. H. Grein, M. E. Flatte, J. T. Olesberg, S. A. Anson, L. Zhang, and T. F. Boggess, J. Appl. Phys. **92**, 7311 (2002).
[32] F. Szmulowicz, Phys. Rev. B **54**, 11 539 (1996); **57**, 9081 (1998); Superlattices Microstruct. **22**, 295 (1997); Eur. J. Phys. **18**, 392 (1997); Am. J. Phys. **65**, 1009 (1997).
[33] G. Bastard, *Wave Mechanics Applied to Semiconductor Heterostructures* (Wiley, New York, 1988).

[34] G. Bastard, J. A. Brum, and R. Ferreira, in *Solid State Physics: Semiconductor Heterostructures, and Nanostructures*, edited by H. Ehrenreich and D. Turnbull, Vol. 44 of *Solid State Physics* (Academic, New York, 1991).
[35] O. Krebs and P. Voisin, Phys. Rev. Lett. **77**, 1829 (1996).
[36] C. Cortez, O. Krebs, and P. Voisin, Eur. Phys. J. B **21**, 241 (2001).
[37] L. Vervoort, R. Ferreira, P. Voisin, Semicond. Sci. Technol. **14**, 227 (1999).
[38] L. Vervoort, R. Ferreira, and P. Voisin, Phys. Rev. B **56**, 12744 (1997).
[39] O. Krebs, W. Seidel, J. P. Andre, D. Bertho, C. Jouanin, and P. Voisin, Semicond. Sci. Technol. **12**, 938 (1997).
[40] H.-R. Trebin, U. Rössler, and R. Ranvaud, Phys. Rev. **20**, 686 (1979).
[41] G. L. Bir and G. E. Pikus, *Symmetry and Strain-Induced Effects in Semiconductors* (Wiley, New York, 1974).
[42] E. L. Ivchenko, A. Yu. Kaminski, and U. Rössler, Phys. Rev. B **54**, 5852 (1996).
[43] U. Rössler and J. Kainz, Solid State Commun. **121**, 313 (2002).
[44] E. L. Ivchenko, A. A. Toporov, and P. Voisin, Phys. Solid State **40**, 1748 (1998).
[45] E. L. Ivchenko and M. O. Nestoklon, Zh. Eksp. Teor. Fiz. **121**, 747 (2002) [JETP **94**, 644 (2002)].
[46] E. L. Ivchenko, A. Yu. Kaminskii, and I. L. Aleiner, JETP **77**, 609 (1993); E. L. Ivchenko and I. L. Aleiner, JETP Lett. **55**, 692 (1992).
[47] B. A. Foreman, Phys. Rev. Lett. **81**, 425 (1998); Phys. Rev. B **54**, 1909 (1996).
[48] M. G. Burt, J. Phys.: Condens. Matter **4**, 6651 (1992).
[49] Takhtamirov and Volkov (private communications).
[50] E. E. Takhtamirov and V. A. Volkov, Pis'ma Zh. Eksp. Teor. Fiz. **77**, 612 (2000) [JETP **71**, 422 (2000)].
[51] E. E. Takhtamirov and V. A. Volkov, Zh. Eksp. Teor. Fiz. **117**, 1221 (2000) [JETP **90**, 1063 (2000)].
[52] E. E. Takhtamirov and V. A. Volkov, Zh. Eksp. Teor. Fiz. **116**, 1843 (1999) [JETP **89**, 1000 (1999)].
[53] K. Kowalik, A. Kudelski, J. A. Gaj, T. Wojtkowicz, O. Krebs, and P. Voisin, Solid State Commun. **126**, 467 (2003).
[54] M. E. Twigg, B. R. Bennett, P. M. Thibado, B. V. Shanabrook, and L. J. Whitman, Philos. Mag. A **7**, 7 (1998), and references therein.
[55] D. W. Stokes, R. L. Forrest, J. H. Li, S. C. Moss, B. Z. Nosho, B. R. Bennett, L. J. Whitman, and M. Goldenberg, J. Appl. Phys. **93**, 311 (2003).
[56] H. J. Haugan, F. Szmulowicz, and G. J. Brown, Appl. Phys. Lett. (2004, to be published); MRS Symp. Proc. **799**, Z5.31 (2004).
[57] J. F. Cracknell, *Group Theory and Electronic Energy Bands in Solids* (Wiley, New York, 1969).
[58] S. D. Ganichev, U. Rössler, W. Prettl, E. L. Ivchenko, V. V. Belkov, R. Neumann, K. Brunner, and G. Abstreiter, Phys. Rev. B **66**, 075328 (2002).
[59] D. L. Smith and C. Mailhiot, Phys. Rev. B **33**, 8345 (1986).
[60] The theory can be easily extended by adding diagonal terms to the IF interaction matrix, Eq. (1b), to account for nonabrupt IF effects as discussed by Takhtamirov and Volkov, Ref. 52.
[61] E. Merzbacher, *Quantum Mechanics*, 2nd ed. (Wiley, New York, 1970), p. 323.
[62] L. R. Ram-Mohan, K. H. Yoo, and R. L. Aggarwal, Phys. Rev. B **38**, 6151 (1988).
[63] *Numerical Data and Functional Relationships in Science and Technology*, edited by O. Madelung, Vol. 17a-b, Group III of Landolt-Bornstein (Springer, New York, 1982); Chris G. Van de Walle, Phys. Rev. B **39**, 1871 (1989).
[64] L. L. Chang, N. J. Kawai, G. A. Sai-Halasz, R. Ludeke, and L. Esaki, Appl. Phys. Lett. **35**, 939 (1979).